Okhotsk Sea and Polar Oceans Research 2 (2018) 1-6

Article

An algorithm for estimating sea-ice type from AMSR-E data in the Beaufort Sea

Yasuhiro TANAKA[1], Kazutaka TATEYAMA[1] and Seita HOSHINO[2]

[1] *School of Engineering, Kitami Institute of Technology, Kitami, Hokkaido, Japan*
[2] *Graduate School of Engineering, Kitami Institute of Technology, Kitami, Hokkaido, Japan*

(Received September 20, 2017; Revised manuscript accepted November 29, 2017)

Abstract

This paper evaluates the validity of an algorithm for estimating sea-ice type from the Advanced Microwave Scanning Radiometer – Earth observing system data (AMSR-E ice type). We compared sea-ice age data on National Snow and Ice Data Center and AMSR-E ice type. The results show an agreement rate > 80% over October–April. This suggests that the algorithm for AMSR-E ice type is valid for distinguishing between first-year ice and multiyear ice during October–April, although the algorithm is affected by major factors such as snow depth and air temperature.

Key words: sea ice, ice type, Arctic Ocean, passive microwave, AMSR-E

1. INTRODUCTION

Sea ice is an essential component of the climate system. The Arctic sea-ice extent in September has accelerated from a rate of ice loss of 36,000 km^2 per year over 1979–1996 to 130,000 km^2 per year over 1997–2014 (Serreze and Stroeve, 2015). Additionally, winter ice volume retrieved using Ice, Cloud, and land Elevation Satellite (ICESat) and multiyear ice (MYI) extent retrieved using the Special Sensor Microwave Imager (SSM/I) decreased 21% in the 6 years over 2003–2008 and 15.6% per year over 1979–2010 (Kwok *et al.*, 2009; Comiso, 2012). This means that Arctic ice thickness has declined.

Heat flux between the atmosphere and ocean for thinner ice was 2.3 times greater than that for thicker ice (Maykut *et al*., 1982). This result is similar to heat flux estimates based on Surface Heat Budget of the Arctic Ocean observations (Lindsay *et al*., 2003). Thus, the distributions of ice type and thickness are important factors for understanding heat flux through sea ice.

Studies have estimated ice thickness distributions by field measurements, submarines, satellites observation such as Microwave Imaging Radiometer with Aperture Synthesis, and ice motion modeling (e.g., Melling and Riedel, 1995; Fowler *et al*., 2004; Rothrock *et al*. 2008; Laxon *et al*., 2013). However, these observations are limited in spatial and temporal coverage.

Satellite passive microwave sensors are not affected by cloud cover and can be used to observe the entire Arctic during night and day. Iwamoto *et al*. (2014) developed a new algorithm for estimating thin ice thickness in the Arctic Ocean using Advanced Microwave Scanning Radiometer-Earth observing system (AMSR-E) data. However, it is difficult to estimate ice thickness in the Arctic Ocean with MYI. Moreover, Krishfield *et al*. (2014) proposed an algorithm for estimating ice type (and thickness) using AMSR-E data (AMSR-E ice type) for the Beaufort Sea. However, the algorithm for estimating AMSR-E ice type (AMSR-E ice-type algorithm) has yet to be evaluated.

We evaluated an AMSR-E ice-type algorithm that distinguishes between first-year ice (FYI) and MYI. MYI was second-year or older ice in our study. An examination of ice thickness results is underway in a separate paper.

2. DATA

Table 1 summarizes specifications of data products used in the present study. Daily mean brightness temperature (T_B) in the AMSR-E/Aqua Daily L3 product are provided by the National Snow and Ice Data Center (NSIDC). The 6.9 GHz channel data with both vertical (V) and horizontal (H) polarization, and 18.7, 23.8, and 36.5 GHz (V) channel data were used to estimate AMSR-E ice type and melt pond fraction (MPF).

Table 1. Specifications of data products

Data products	Parameters	Gridding interval	Temporal Coverage	Temporal resolution
AMSR-E/Aqua Daily L3	T_B	25 km x 25 km	Jun. 2002 to Oct. 2011.	Daily
MEaSUREs Arctic Sea Ice Characterization	Sea Ice Age	25 km x 25 km		
Global Sea Ice Concentration Climate Data Record v2.0	Sea Ice concentration	25 km x 25 km		
CFSR	Air temperature Snow depth	0.5° x 0.5°	Jun. 2002 to Dec. 2010	6 hourly
CFSv2			April. 2011 to Oct. 2011	

Sea-ice age in the NASA Making Earth System Data Records for Use in Research Environments Arctic Sea Ice characterization provided by NSIDC (NSIDC ice age) were used to compare AMSR-E ice type because

projection of the two data sets is the same. The ice age output the oldest ice age values on each grid cell and between FYI and 10th-year ice, based on satellite remote sensing-based sea-ice motion data. This means that ice age was omitted the passages over the Canadian Arctic Archipelago. This remote sensing-based age is similar to buoy-derived age produced by Rigor and Wallace (2004) as shown in NSIDC.

Sea-ice concentration data in Global Sea Ice Concentration Climate Data Record (version 2.0) are available at the EUMETSAT Ocean and Sea Ice Satellite Application Facility (OSISAF), and include the product user manual (Sørensen *et al*., 2017) and validation report (Kreiner *et al*., 2017). The biases of the sea-ice concentration data in summer and other season were −5% and −1–−2%, respectively, compared to National Ice Center sea-ice charts. These data were retrieved from the European Space Agency Climate Change Initiative Sea Ice (phase 2) Low Frequency channels algorithm, which improved on the OSISAF "hybrid" algorithm (itself a combination of Bootstrap Freq-Mode and Bristol algorithms) (Tonboe *et al*., 2016).

The Climate Forecast System (CFS) Reanalysis and CFS Version 2 (CFSv2) data for 2-m air temperature and snow depth are produced and provided by the National Centers for Environmental Prediction (NCEP). These data were used to examine the effect of depth and air temperature on the AMSR-E ice-type algorithm. A NSIDC grid cell was taken from the nearest CFS grid cell. The snow depth in CFSs had a positive bias during winter (10–20 cm) and spring (5–25 cm), a negative bias during summer (−25–0 cm) and autumn (−5–10 cm), compared to the buoy-derived snow depth (Sato and Inoue, 2017).

3. AMSR-E ICE TYPE ALGORITHM

The AMSR-E ice-type algorithm for the Beaufort Sea (including background) is explained in detail in Krishfield *et al*. (2014) and is outlined here. Hereafter, V-polarization at frequency 18.7 GHz is expressed as T_{B18V}, and this convention is also used for the other channels. Cavalieri *et al*. (1984) reported that the gradient ratio (*GR*) between T_{B19V} and T_{B37V} in SSM/I data ($GR_{\mathrm{19V–37V}}$) is valid for distinguishing between FYI and MYI in the NASA team standard ice algorithm for the Arctic Ocean. This is because MYI has much lower salinity and less moisture (Ulaby *et al*., 1982).

Krishfield *et al*. (2014) defined the *GR* between T_{B18V} and T_{B36V} in AMSR-E data ($GR_{\mathrm{18V–36V}}$), which was compared with shipborne electromagnetic induction device thickness during late summer. $GR_{\mathrm{18V–36V}}$ is sensitive to change in ice thickness in MYI areas. This suggests that $GR_{\mathrm{18V–36V}}$ varies with ice temperature at penetration depths for 18.7 and 36.5 GHz channels, as well as snow depth over sea ice. $GR_{\mathrm{18V–36V}}$ accuracy was also examined by comparison with daily-average ice draft data from the upward looking sonar (ULS draft) mounted on the Beaufort Gyre observing system mooring. Thickness derived from $GR_{\mathrm{18V–36V}}$ is in agreement with the ULS draft in September. However, there is no agreement for other months. Therefore, *GR* was improved by using T_{B06V} and T_{B36V}, because the difference between 6 and 36 GHz is the largest, and so it is the most sensitive to the ULS draft. *GR* between T_{B06V} and T_{B36V} ($GR_{\mathrm{06V–36V}}$) are defined by the following equation.

$$GR_{06V-36V} = \frac{T_{B06V} - T_{B36V}}{T_{B06V} + T_{B36V}} \tag{1}$$

Using this definition of $GR_{\mathrm{06V–36V}}$, the range of $GR_{\mathrm{06V–36V}} \geq -0.025$ was considered FYI, and $GR_{\mathrm{06V–36V}} < -0.025$ was considered MYI.

4. RESULTS

To evaluate the validity of the AMSR-E ice-type algorithm, we compared NSIDC ice age and AMSR-E ice type and examined their agreement rate. For example, if NSIDC ice age indicated MYI, then the algorithm was correct when AMSR-E ice type indicated MYI. T_{B06V} and T_{B36V} for $GR_{\mathrm{06V–36V}}$ was affected by melt ponds during summer (May–August) (Tanaka *et al*., 2016). If the MPF (Eq. 2) was > 20%, grid cells were not included in the analysis.

$$MPF = 15.2 - 158.9\left(\frac{T_{B06H} - T_{B89V}}{T_{B06H} + T_{B89V}}\right) \tag{2}$$

Figure 1 shows seasonal change of mean agreement rate between NSIDC ice age and AMSR-E ice type. The maximum rate was 98% at the end of September. The rate decreased to 86% in December and was nearly constant from January to April. Subsequently, the rate in May decreased to 60%, and standard deviation of the rate also increased. Moreover, the number of grid cells declined during summer because cells with MPF > 15% were not included.

Figure 2 shows examples of the distributions of both NSIDC ice age and AMSR-E ice type. These distributions on 1 January and 1 April were similar. Agreement rates were respectively 91% and 90% on those dates. Although the rate was 88% on 1 September, it is difficult to understand the distribution of AMSR-E ice type across the entire Arctic Ocean. Additionally, FYI grid cells were situated between MYI grid cells in the distribution of NSIDC ice age (Figs. 2a, 2c, and 2e). This characteristic was not found in the distribution of AMSR-E ice type (Figs. 2b, 2d, and 2f).

Figure 3 shows seasonal change of mean $GR_{\mathrm{06V\text{-}36V}}$, air temperature, and snow depth. During the high

agreement rate (October–April), the difference between mean $GR_{06V\text{-}36V}$ of FYI and MYI was 0.045. However, standard deviations of the rate for FYI and MYI were 0.035 and 0.03, respectively. This means that the change of $GR_{06V\text{-}36V}$ varied by year. The change of snow depth and air temperature behaved similarly.

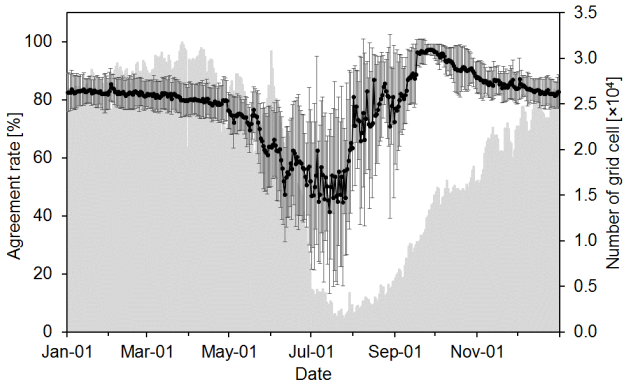

Fig. 1 Seasonal change of mean agreement rate between NSIDC ice age and AMSR-E ice type over the Beaufort Sea during 2002–2011, with standard deviations (vertical lines). Gray bars show number of grid cells.

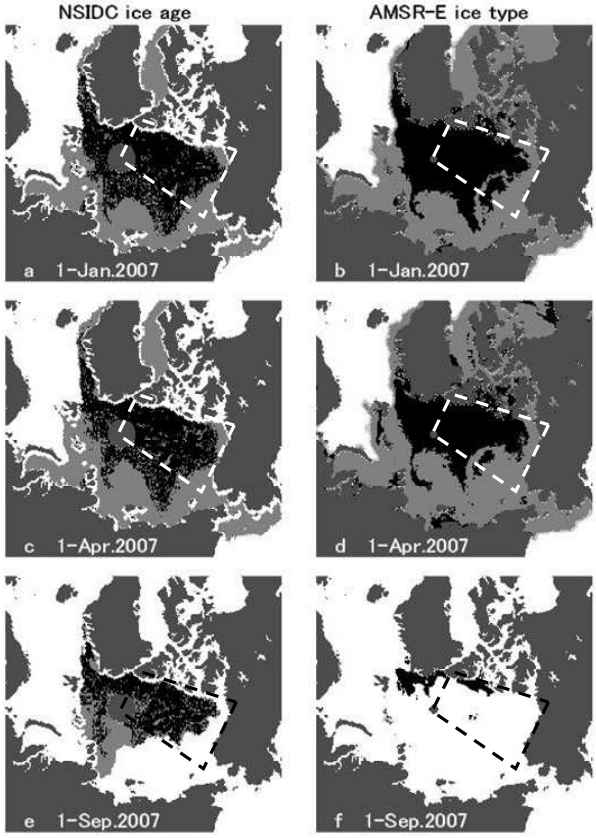

Fig. 2 Examples of NSIDC ice age (left panels) and AMSR-E ice type (right panels) distributions for January, April, and September 2007. Black, light gray, dark gray, and white are multiyear ice, first-year ice, land, and missing grid cells, respectively. A missing grid cell means > 20% melt pond fraction or open water (< 20% sea-ice concentration). Analysis area in this study exists inside the trapezoid.

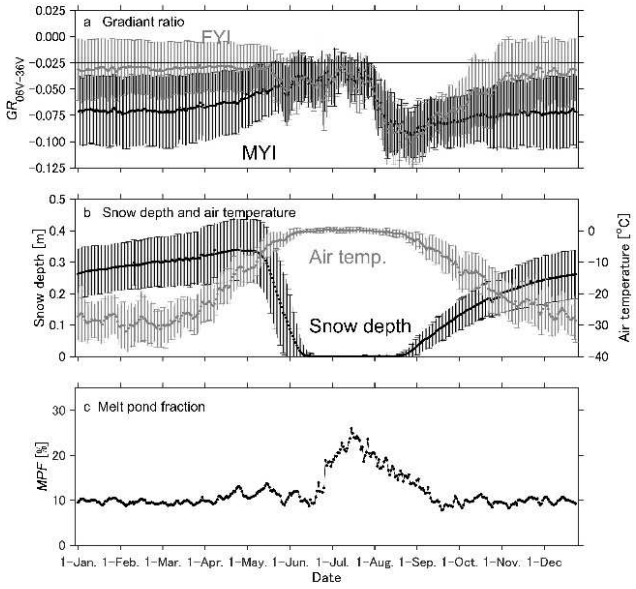

Fig. 3 Seasonal change of mean (a) $GR_{06V\text{-}36V}$ from calculated AMSR-E data, (b) air temperature and snow depth from CFSs with standard deviations (vertical lines), and (c) melt pond fraction from calculated AMSR-E data over the period 2002–2011 in the Beaufort Sea. Multiyear ice (MYI) and first-year ice (FYI) in panel (a) are from NSIDC ice age.

5. DISCUSSION

The agreement rate between NSIDC ice age and AMSR-E ice type is > 80 % for October to April. This demonstrates that the AMSR-E ice-type algorithm is valid for distinguishing FYI from MYI.

The agreement rate for 1 September is higher than that in other months. However, estimated areas of AMSR-E ice type (especially minimum sea-ice extent in September 2007 over the years 2002–2011) were limited by the effect of MPF (Fig. 2f). This indicates an unacceptable agreement rate in summer and September.

We now address the causes of the disagreement between NSIDC ice age and AMSR-E ice type. Eicken *et al*. (2002) and Perovich *et al*. (2009) reported that the salinity of thicker FYI (> 70 cm) is similar to that of MYI. Additionally, T_{B36V} for $GR_{06V–36V}$ was sensitive to the difference between FYI and MYI salinities. We believe that the AMSR-E ice-type algorithm regards thicker FYI as MYI.

The AMSR-E ice-type algorithm determines the dominant ice type in a grid cell. In contrast, NSIDC ice age outputs the oldest ice age in a grid cell if that cell includes ice of different ages. This does not necessarily output the dominant NSIDC ice age in a grid cell. Therefore, a cause for the disagreement may be the difference of determination method for AMSR-E ice type and NSIDC ice age.

We considered the effect of $GR_{06V–36V}$ on snow depth and air temperature. Relationships between $GR_{06V–36V}$

and snow depth and air temperature were examined as shown in Table 2. T_{B36V} decreased with snow depth (Eppler *et al*., 1992). The relationship between $GR_{06V–36V}$ and snow depth tends to be strong for FYI in December (r = −0.51) and MYI in October (r = −0.53). As an example, $GR_{06V–36V}$ decreases with the increasing snow depth in October (Fig. 4a). Then, the increase of snow depth is 0.1 m per month (Fig. 3b). This suggests that change of snow depth affects $GR_{06V–36V}$. However, the increase of snow depth (0.01 m per month) during January–April is less (Fig. 3b). The relationship between $GR_{06V–36V}$ and snow depth is also weak (Table 2). According to Sato and Inoue (2017), snow depth in CFS data has a positive bias during winter and spring, greater than that during autumn. Therefore, we believe that the biases affect the relationship between $GR_{06V–36V}$ and snow depth as shown in Table 2.

Table 2. Correlation coefficients (r) and p-values between $GR_{06V-36V}$, and snow depth and air temperature for first-year ice (FYI) and multiyear ice (MYI) in the Beaufort Sea.

	Snow depth				Air temperature			
	FYI		MYI		FYI		MYI	
Month	*r*	*p*	*r*	*p*	*r*	*p*	*r*	*p*
1	-0.04		0.30	< 0.001	0.02	0.45	-0.22	0.45
2	0.05		0.31		-0.21	0.45	-0.29	0.45
3	0.43		0.50	0.35	-0.08	0.22	-0.02	0.22
4	0.25	< 0.001	0.32		-0.49		0.05	
10	-0.32		**-0.53**	< 0.001	0.27	< 0.001	**0.67**	< 0.001
11	-0.38		0.11		**0.51**		**0.93**	
12	**-0.51**		0.18		-0.40		0.28	

T_Bs is affected by the relationship between surface temperature and air temperature. The relationship between $GR_{06V–36V}$ and air temperature tended to be strong for FYI (r = 0.51) and MYI (r = 0.93) in November. As shown in Fig. 4b, $GR_{06V–36V}$ increased with air temperature. However, the relationship between $GR_{06V–36V}$ and air temperature was weak during December–April. This suggests that the increase of air temperature (3 °C per month) was less than that during October and December (7 °C per month). Thus, $GR_{06V–36V}$ is affected by snow depth and air temperature in addition to ice type.

$GR_{06V–36V}$ tended to increase in October and November (Fig. 5). Trends of MYI in October and November were 0.0031 and 0.017 per year, respectively. Moreover, the differences between $GR_{06V–36V}$ for FYI and MYI were greater than those in November. These results suggest that the threshold for estimating AMSR-E ice type changes monthly and yearly. The threshold may need further improvement if ice types are retrieved using AMSR2 data since 2012.

The aforementioned findings will serve as a basis for further understanding of essential effects on the AMSR-E ice-type algorithm. Kimura *et al*. (2013) advanced the possibility that the ice thickness distribution in spring is affected by the redistribution of ice floes in winter. This is important for potential improvement in prediction of the summer ice area in spring by investigating winter ice motion. Moreover, information of sea-ice type in spring is useful for a prediction model of melt pond expansion (Eicken *et al*., 2004). This is because melt ponds in summer differ in their range of expansion on FYI and MYI and are a major influence on the ice–albedo feedback mechanism (e.g., Flocco *et al*., 2007; Schröder *et al*., 2014). Thus, the AMSR-E ice-type algorithm will also be useful for these predictions.

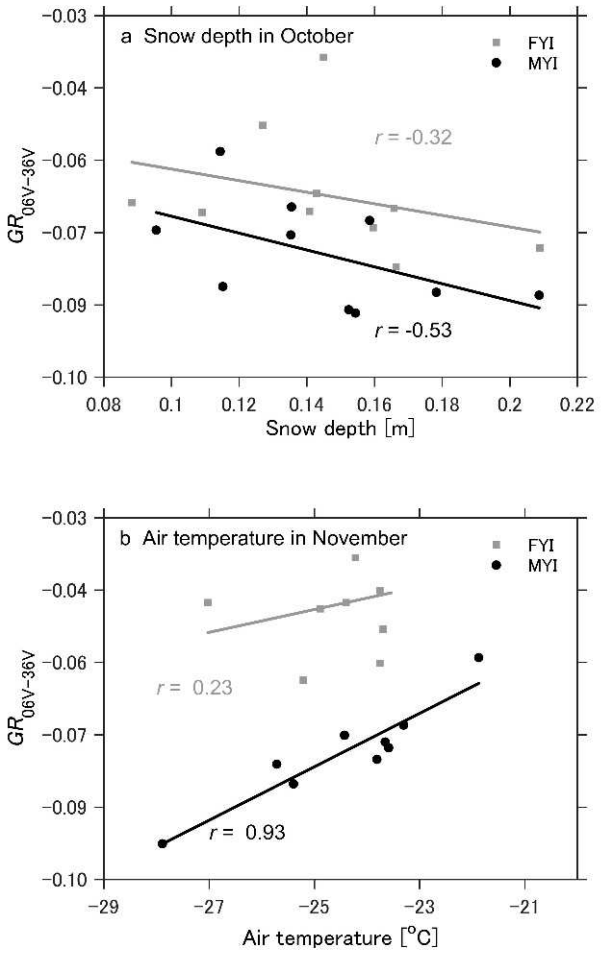

Fig. 4 Relationship between $GR_{06V-36V,}$ and (a) snow depth in October and (b) air temperature in November over the period 2002–2011. r denotes the correlation coefficient for the Beaufort Sea. Solid lines in these panels show regression lines. These relationships are statistically significant at the 99.9% confidence level. FYI and MYI are first-year ice and multiyear ice, respectively.

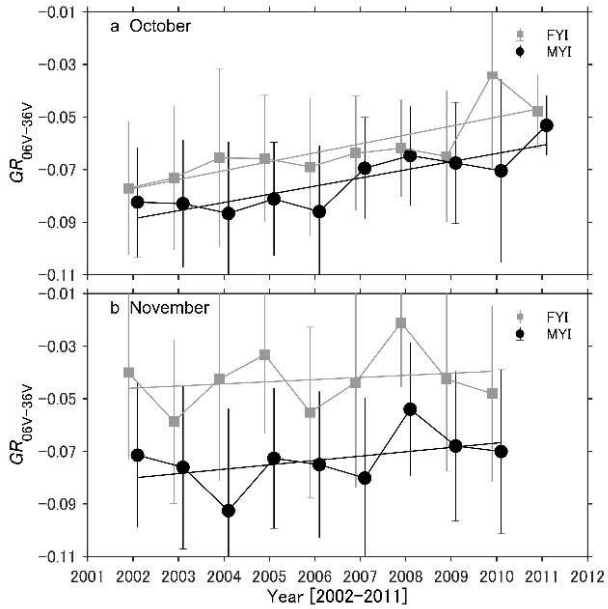

Fig. 5 Time series of $GR_{06V-36V}$ in (a) October and (b) November from 2002–2011 with standard deviations (vertical lines) in the Beaufort Sea. Solid lines in these panels show regression lines. FYI and MYI are first-year ice and multiyear ice, respectively.

6. CONCLUSIONS

We compared NSIDC ice age and AMSR-E ice type to evaluate the AMSR-E ice type algorithm. The study focused on area and period in the Beaufort Sea during October–April 2002–2011.

The agreement rate between NSIDC ice age and AMSR-E ice type exceeded 80% from October to April. This rate increased to 86% in December and was constant from January to April. The distributions of AMSR-E ice type in January and April 2007 were in agreement with those of NSIDC ice age. We believe that the major causes of disagreement were the following: (1) The algorithm regarded thicker FYI as MYI, and (2) snow depth and air temperature affected $GR_{06V–36V}$.

Although the AMSR-E ice-type algorithm was mainly influenced by the two factors above, the algorithm was valid for distinguishing FYI from MYI during October–April. Our findings will contribute to the improvement of algorithm accuracy. This will support accurate prediction of sea-ice cover, type and thickness, as well as the model of melt pond expansion.

ACKNOWLEDGMENTS

This study was supported by the Arctic Challenge for Sustainability (ArCS) Project. We appreciate Jun Inoue for helpful conversations during the course of this work. The products for brightness temperature and sea-ice age were obtained from the National Snow and Ice Data Center (NSIDC; http://nsidc.org/). The products for snow depth and air temperature were provided by the National Centers for Environmental Prediction Climate Forecast System Reanalysis (https://climatedataguide.ucar.). The global sea ice concentration climate data record 1978–2015 (version 2.0) was provided from the EUMETSAT Ocean and Sea Ice Satellite Application Facility (http://osisaf.met.no). We are grateful to Stefan Kern and Steinar Eastwood for their help with the products. We thank Steven Hunter, M.S, from Edanz Group (www.edanzediting.com/ac) for editing a draft of this manuscript.

REFERENCES

Cavalieri, D. J., P. Gloersen, and W. J. Campbell (1984): Determination of sea ice parameters with the NIMBUS 7 SMMR. *J. Geophys. Res.*, **89**: D4, 5355–5369.

Comiso, J. C. (2012): Large decadal decline of the Arctic multiyear ice cover. *J. Climate*, **25**(4), 1176–1193, doi: 10.1175/JCLI-D-11-00113.1.

Eppler, D. T. and 6 others (1992), Passive microwave signatures of sea ice, in Microwave Remote Sensing of Sea Ice. *Geophys. Monogr. Ser*., **68**, edited by F. D. Carsey, 47–71, AGU, Washington, D. C.

Eicken, H. and 3 others (2002): Tracer studies of pathways and rates of meltwater transport through Arctic summer sea ice. *J. Geophys. Res.*, **107**: C10, 8046, doi:10.1029/2000JC000583

Eicken, H. and 4 others (2004): Hydraulic controls of summer Arctic pack ice albedo. *J. Geophys. Res.*, **109**, C08007.

Flocco, D., and D. L. Feltham (2007): A continuum model of melt pond evolution on Arctic sea ice. *J. Geophys. Res.*, **112**: C08016.

Fowler, C., W. J. Emery, and J. Maslanik. (2004): Satellite-derived evolution of Arctic sea ice Age: October 1978 to March 2003. *Geoscience and Remote Sensing Letters, IEEE*, **1**(2), 71-74, doi: 10.1109/LGRS.2004.824741.

Iwamoto, K., K. I. Ohshima, and T. Tamura (2014), Improved mapping of sea ice production in the Arctic Ocean using AMSR-E thin ice thickness algorithm. *J. Geophys. Res. Oceans*, **119,** 3574–3594, doi:10.1002/ 2013JC009749.

Kimura, N. and 3 others (2013), Influence of winter sea ice motion on summer ice cover in the Arctic. *Polar Res.*, **32**, 2,0193, doi:10.3402/polar.v32i0.20.

Kreiner and 7 others (2017): Validation report for Global sea ice concentration reprocessing. EUMETSAT OSISAF Products OSI-450, Document version: 2.0.

Krishfield, R. A. and 6 others (2014): Deterioration of perennial sea ice in the Beaufort Gyre from 2003 to 2012 and its impact on the oceanic freshwater cycle. *J. Geophys. Res. Oceans*, **119**, 1271–1305, doi:10.1002/2013JC008999.

Kwok R., Cunningham G.F., Wensnahan M., Rigor I., Zwally H.J. & Yi D. 2009. Thinning and volume loss of the Arctic Ocean sea ice cover: 2003–2008. *J. Geophys. Res. Oceans*, **114**: C07005, doi: 10.1029/2009JC005312.

Lindsay, R.W. (2003): Changes in the modeled ice thickness distribution near the Surface Heat Budget of the Arctic Ocean (SHEBA) drifting ice camp. *J. Geophys. Res.*, **108**: C6, 3194.

Laxon, S. W. and 14 others (2013): CryoSat-2 estimates of Arctic sea ice thickness and volume. *Geophys. Res. Lett.*, **40**, 732–737.

Maykut, G. A. (1982): Large-scale heat exchange and ice production in the central Arctic. *J. Geophys. Res.*, **87**: C10, 7971–7984.

Melling, H. and Riedel, D. A. (1995): The underside topography of sea ice over the continental shelf of the Beaufort

Sea in the winter of 1990. *J. Geophys. Res.*, **100**: C7, 13,641–13,653.
Perovich, D. K. and 7 others (2009): Transpolar observations of the morphological properties of Arctic sea ice. *J. Geophys. Res.*, **114**, C00A04, doi:10.1029/2008JC004892.
Rigor, I. G., and J. M. Wallace (2004): Variations in the age of Arctic sea-ice and summer sea-ice extent. *Geophys. Res. Lett.*, **31**, L09401, doi:10.1029/2004GL019492.
Rothrock D.A., Percival D.B., and Wensnahan M. (2008): The decline in Arctic sea-ice thickness: separating the spatial, annual, and interannual variability in a quarter century of submarine data. *J. Geophys. Res. Oceans*, **113**: C05003, doi: 10.1029/2007JC004252.
Sato, K. and J. Inoue (2017): Comparison of Arctic sea ice thickness and snow depth estimates from CFSR with in situ observations. *Clim. Dyn.*, doi: 10.1007/s00382-017-3607-z.
Serreze, M. C. and J. Stroeve (2015): Arctic sea ice trends, variability and implications for seasonal ice forecasting. Philos. *Trans. Roy. Soc. London*, **373**, 20140159, doi:10.1098/rsta.2014. 0159.
Sørensen, A. M., Lavergne. T., and Eastwood S. (2017): Global Sea Ice Concentration Reprocessing. Product *User Manual*, *EUMETSAT OSISAF, Document version*: 1.0, Data set version: 2.0.
Schröder, D. and 3 others (2014): September Arctic sea-ice minimum predicted by spring melt-pond fraction. *Nature Climate Change*, **4**, 353–357.
Tanaka, Y., K. Tateyama, T. Kameda, and J. K. Hutchings (2016): Estimation of melt pond fraction over high-concentration Arctic sea ice using AMSR-E passive microwave data. *J. Geophys. Res. Oceans*, **121**, 7056–7072, doi:10.1002/2016JC011876.
Tonboe, R. T. and 7 others (2016): The EUMETSAT sea ice concentration climate data record. *The Cryosphere*, **10**, 2275-2290, doi:10.5194/tc-10-2275-2016.
Ulaby, F. T., R. K. Moore, and A. K. Fung (1982): Microwave Remote Sensing, Active and Passive, Vol. II - Radar Remote Sensing and Surface Scattering and Emission Theory, 609 pp., Artech House, Inc., Dedham, Massachusetts.

Summary in Japanese
和文要約

AMSR-E データによるボーフォート海の海氷の種類判別手法

田中康弘 [1], 舘山一孝 [1], 星野聖太 [2]

[1] 北見工業大学工学部, [2] 北見工業大学大学院工学研究科

海氷は気候システムの重要な構成要素の一つである. 海氷の種類は, 海氷域における大気–海洋間の熱交換の影響を知るために重要である. 本研究では, 衛星マイクロ波放射計 AMSR-E データによる海氷の種類判別手法の有効性を評価した. この手法による海氷の種類と NSIDC による海氷年齢を比較した結果, 一致率は 10 月から 4 月の間で 80%を示した. これは秋から冬の間, AMSR-E による海氷の種類判別手法が一年氷と多年氷の判別に有効であると考えられる. また, その手法での一年氷と多年氷の判別閾値は, 積雪深や気温に影響されることがわかった. 今後は, 世界最高水準の AMSR2 データによる海氷の種類判別手法の開発を目指す.